# Passive Stall Control in MAVs Using Sinusoidal Leading Edges - Part A

João L. Guerreiro*
*Department of Mechanical Eng., Instituto Superior Técnico, Lisbon, Portugal*

**The objective of the present work is to investigate the application of a sinusoidal leading edge to the design of MAVs. Wind tunnel tests of wings with low aspect ratios of 1 and 1.5, rectangular planforms, and 5 distinct leading edges — 4 sinusoidal leading edges and 1 baseline leading edge for each aspect ratio — have been conducted. We have considered Reynolds numbers of 70000 and 140000. For the higher Reynolds number a proper combination of amplitude and wavelength can lead to substantial increases in lift for angles of attack greater than the baseline stall angle. At lower Reynolds numbers the benefits can be extended for low angles of attack, leading to a dramatic increase in the range of operation. The results depend strongly in the aspect ratio. This paper is the first of a series of two papers. In the second paper (Part B), we present the results for yaw angles of 15 and 30 degrees.**

## Nomenclature

| | | |
|---|---|---|
| $\mathcal{AR}$ | = | aspect ratio, $b^2/S$ |
| $b$ | = | wing span |
| $C_D$ | = | drag coefficient, $D/0.5\rho V_\infty^2 S$ |
| $C_L$ | = | lift coefficient, $L/0.5\rho V_\infty^2 S$ |
| $c$ | = | mean chord length |
| $D$ | = | drag force |
| $L$ | = | lift force |
| $Re$ | = | Reynolds number, $\rho V_\infty c/\mu$ |
| $S$ | = | wing area |
| $V_\infty$ | = | freestream velocity |
| $\alpha$ | = | angle of attack, deg |
| $\mu$ | = | viscosity |
| $\rho$ | = | air density |

## I. Introduction

THE interest in micro air vehicles (MAVs) has grown exponentially in the last years motivated by the increasing capability in miniaturize the avionics. Equipped with small video cameras, transmitters and sensors, MAVs are perfect candidates for special limited-duration military and civil missions. Which may include real-time images of battlefields, detection of biological agents, chemical compounds and nuclear materials, surveys of natural disaster areas and monitoring forest fires.[1,2]

Due to the combination of small dimensions and low speeds, MAVs fly at low Reynolds numbers ($< 200000$[3]). In this regime many complicated phenomena take place within the boundary layer. Their lifting surfaces are very susceptible to laminar flow separation, and the laminar bubble that commonly forms can have a dramatic effect on the aerodynamic performance. This becomes particularly evident when the long term goal is to develop a vehicle with a wing span of 8 cm that can fly at speeds between 30 to 65 km/hr,[1] which identifies at the best (i.e., when the chord length is equal to the wing span) maximum Reynolds numbers between 45000 and 100000. Plus, the stability and control problems associated with the low moments of inertia, small weight, and wind gusts, presents plenty of challenges.[3]

Here, we propose a passive method, inspired in the humpback whale pectoral flippers (*Megaptera novængliæ*), to control stall and increase the range of operation. The humpback whale is extremely agile and it can perform admirable turning manuevers to catch prey.[4] Its pectoral flippers have high aspect ratios ($\approx 6$), being the longest among the cetaceans, and have an elliptical planform. However, its most notable feature is the unusual leading edge, made up of several tubercles which gives it an aspect resembling a sinusoidal pattern.[5] Figure 1 shows a photograph of the humpback whale and its pectoral flipper.

The first wind tunnel experiments conducted by Miklosovic et al.[6] used a scale model of an idealized humpback whale flipper. They showed a delay stall angle by about 40%, while increasing the maximum lift and reducing the drag over a portion of the operational envelope. The Reynolds number was about 500000, estimated to be half of the value of an adult humpback whale. Subsequently, Stanway[7] tested a similar scale model at Reynolds number between 45000 e 120000. He reported a delay in stall angle, however, the maximum lift increased only for the higher Reynolds number. PIV (Particle Image Velocimetry) flow visualization suggests that two longitudinal counter-rotative vortices are formed at each protuberance, in a manner similar to the leading-edge vortices of a delta wing; by energizing the flow they delay stall.

In another type of approach, Miklosovic et al.[8] (at $Re \approx 275000$) and Johari et al.[9] (at $Re \approx 183000$) tested infinite models in order to study the fundamental nature of the resulting flow from the presence of protuberances. The results were substancially different from the finite scale models. There is an overall increase in drag and the models with a sinusoidal leading-edge stalls first. However, the stall behavior is better (i.e. more gradual) and the lift coefficients are still higher beyond the point of stall of the baseline model (i.e. without tubercles). Tuft visualization[9] showed that the flow separates first at the troughs between the adjacent protuberances while it is kept attached over the peaks at angles of attack higher than the baseline model stall. Another interesting finding from Johari et al. is that the amplitude of the protuberances had a much greater effect on the results than the wavelength.

More recently, Pedro and Kobayashi[10] used a DES (Detached Eddy Simulation) formulation to numerically simulate the experience of Miklosovic et al.[6] They concluded that the longitudinal structures of vortices not only delay the trailing-edge separation that takes place in the inboard section — where the local Reynolds numbers are higher ($> 500000$) — as they prevent the propagation of the leading edge separation that occurs in the outboard section — where the local Reynolds number are lower ($< 200000$)— from moving towards the root.

The primary goal of this study is to investigate the applicability of this solution to the design of MAVs. Normally, in the development of these vehicles the wing span is a size constraint, so low aspect ratio wings give the largest wing area for higher lift. For that purpose we use a combination of low Reynolds number and low aspect ratio wings with different types of protuberances.

*MSc Student, Department of Mechanical Eng., Instituto Superior Técnico.

**Fig. 1 Humpback whale breaching in the Southern Ocean and a close-up shot of its pectoral flipper (from Ref. 7).**

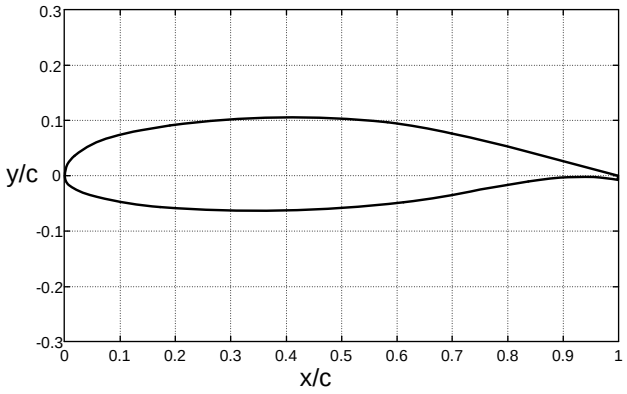


**Fig. 2 NASA LS(1)–0417 profile.**

## II. Experimental Apparatus

### A. Wing Model Configuration

Ten rectangular wings based on the NASA LS(1)–0417 profile (Fig. 2) were machined from duralumin blocks and polished. The surface finish quality, less than 1 $\mu$m RMS roughness height, was measured with a Mitutoyo SJ-201 profilometer.

The models have a mean chord length of 232 mm and they can be divided in two sets accordingly to its aspect ratio of 1 or 1.5. Each set is formed by the baseline model and four models with a sinusoidal leading edge. To define the sine wave, two amplitudes of 0.06c and 0.12c were chosen with two wavelengths of 0.25c and 0.50c. The chosen values are inspired by previous investigations[9] and fall within the range of values associated with the humpback whale pectoral flippers. Figure 3 shows the set of wings with aspect ratio 1.5. The models designation is as follow: the first characters define the type of model (B for baseline model and S for sinusoidal model) and the aspect ratio; the last characters, separated from the previous by a hyphen and used only for the sinusoidal models, refers to its amplitude (L stands for large amplitude, i.e. 0.12c, and S stands for small amplitude, i.e. 0.06c) and the wavelength (analogous, L for 0.5c and S for 0.25c). Table 1 list the dimensions and other geometry parameters for the wing models used in this investigation.

### B. Wind Tunnel and Instrumentation

The experiments were performed in the open-circuit blow-down wind tunnel located at the Department of Mechanical Engineer. The wind tunnel works in the low speed (incompressible) flow regime. The tests can be operated in free jet or in a test section with a square cross-sectional area of 1.35 m $\times$ 0.8 m. Since, we are studying the tridimensional flow that develops around the models, we chose to operate in free jet to reduce the number of corrections to be applied to the results. The test section is precedeed by honeycombs, screens, and a contraction ratio of 3 to 1 to provide uniform low turbulent incoming flow. Over the speed range used, the maximum freestream turbulence intensity is estimated to be 0.15%.

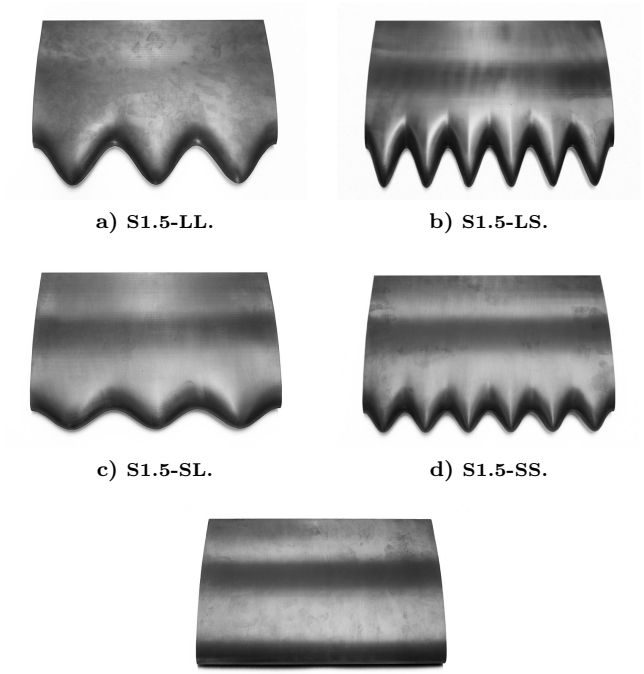

**a) S1.5-LL.** **b) S1.5-LS.**

**c) S1.5-SL.** **d) S1.5-SS.**

**e) B1.5.**

**Fig. 3 Set of wing models with $\mathcal{AR} = 1.5$.**

The aerodynamic forces and moments are transmitted to a six-component Schenck compact balance through the model support. The values measured by the load cells are acquired using a PREMA 5001 digital multimeter of 6 1/2 digits which communicates with the host computer using the GPIB protocol. Scan rates of 5 channels per second can be executed with this system.

### C. Experimental Procedures and Uncertainty

The experiments were conducted at two Reynolds numbers of 70000 and 140000, which are termed the low Reynolds number regime and the moderate Reynolds number regime. The angle of attack was varied from $\alpha = 0$ deg to $\alpha = 30$ deg. After this point, the wings were brought back to $\alpha = 0$ deg to check if hysteresis was present. For each angle of attack we acquired between 15 to 30 samples at an effective scan rate of 0.87 channels per second.

Flow visualization tests were conducted for the B1.5 and S1.5-LL models at a zero yaw angle, using the smoke wire technique and a laser sheet to illuminate the semi-span plan. Still images were obtained during the tests with a digital camera Sony DSLR-A200.

To predict the overall 95% confidence limits for $C_L$ and $C_D$ we followed the procedure given by Coleman and Steele.[11] To estimate the precision uncertainties the standard error for the mean force coefficients at each angle of attack was calculated and multiplied by the two-tailed $t$ value ($t = 2$) for a number of readings greater than 10. These were combined with the estimates of the bias errors to predict the overall 95% confidence limits.

Percentage uncertainties for $C_L$ are on the order of 4.5% for the moderate Reynolds numbers and 5.5% for the low Reynolds numbers. Analogous, percentage uncertainties for $C_D$ are on the order of 20% for the moderate Reynolds numbers; for the low Reynolds numbers are on the order of 30% and 45% for the models with aspect ratios 1.5 and 1, respectively. Therefore only the lift coefficient variation with angle of attack will be presented.

The uncertainty in the angle of attack is estimated to be of the order of 0.2 deg.

**Table 1 Wing model dimensions.**

| Wing | c (mm) | b (mm) | $\mathcal{R}$ | $A$ (mm) | $\lambda$ (mm) |
|---|---|---|---|---|---|
| B1 | 232 | 232 | 1 | – | – |
| S1-LL | 232 | 232 | 1 | 0.12c | 0.50c |
| S1-LS | 232 | 232 | 1 | 0.12c | 0.25c |
| S1-SL | 232 | 232 | 1 | 0.06c | 0.50c |
| S1-SS | 232 | 232 | 1 | 0.06c | 0.25c |
| B1.5 | 232 | 348 | 1.5 | – | – |
| S1.5-LL | 232 | 348 | 1.5 | 0.12c | 0.50c |
| S1.5-LS | 232 | 348 | 1.5 | 0.12c | 0.25c |
| S1.5-SL | 232 | 348 | 1.5 | 0.06c | 0.50c |
| S1.5-SS | 232 | 348 | 1.5 | 0.06c | 0.25c |

**Table 2 Aerodynamic characteristics of the wings with aspect ratio 1.**

| Wing | $C_{L_{\alpha=0^\circ}}$ | $C_{L_{max}}$ | $\alpha_{C_{L_{max}}}$, deg | $\alpha_{stall}$, deg |
|---|---|---|---|---|
| B1 | 0.120 | 0.79 | 30 | 21 |
| S1-LL | 0.142 | 0.82 | 30 | – |
| S1-LS | 0.136 | 0.75 | 30 | 20 |
| S1-SL | 0.143 | 0.78 | 27 | 27 |
| S1-SS | 0.140 | 0.79 | 30 | – |

## III. Experimental Results

The measured lift for the baseline and sinusoidal leading edge models are presented next. We start by presenting the results at the moderate Reynolds number; first for the wings of aspect ratio 1 and afterwards for the wings of aspect ratio 1.5. Then the results are discussed and compared. The procedure is repeated for the low Reynolds number flow.

For simplicity, the models with and without protuberances along the leading edge are termed sinusoidal models and baseline models.

### A. Moderate Reynolds Number

#### 1. *Aspect ratio 1*

Figure 4 shows the lift coefficient variation with angle of attack for all the models.

The baseline model $C_L$ keeps increasing at a reasonable linear rate up to $\alpha = 21^\circ$, beyond which it is slightly reduced (stall). However, further increases in incidence lead to greater lift values. The maximum $C_L$ of 0.79 is only reached at the maximum angle of attack tested ($\alpha_{max} = 30^\circ$) and is approximately 13% higher than the value at stall.

For $\alpha \leq 20^\circ$, the behavior of the sinusoidal models is very similar to the baseline model, despite the lower slope ($dC_L/d\alpha$), which ultimately introduces a penalization in lift coefficient. Still they have more favorable stall characteristics. The S1-LS model — the one that moves away more from the baseline leading edge geometry — is the first to stall at $\alpha = 20^\circ$, but it has a more gradual and softer stall then the baseline model. The S1-SL — the one that is closer to the baseline leading edge geometry — stalls at a much higher angle of attack, $\alpha = 27^\circ$. The other two models do not stall. In the poststall regime the more evident feature is the reduction in lift of the S1-LS model. On the other hand the S1-LL model leads to a consistent gain, nonetheless, very small to be considered relevant.

Table 2 lists the aerodynamic characteristics incuding $C_{L_{\alpha=0^\circ}}$, the maximum $C_L$, angle of maximum $C_L$ and stall angle.

#### 2. *Aspect ratio 1.5*

The data for the wings with aspect ratio 1.5 is shown in Fig. 5.

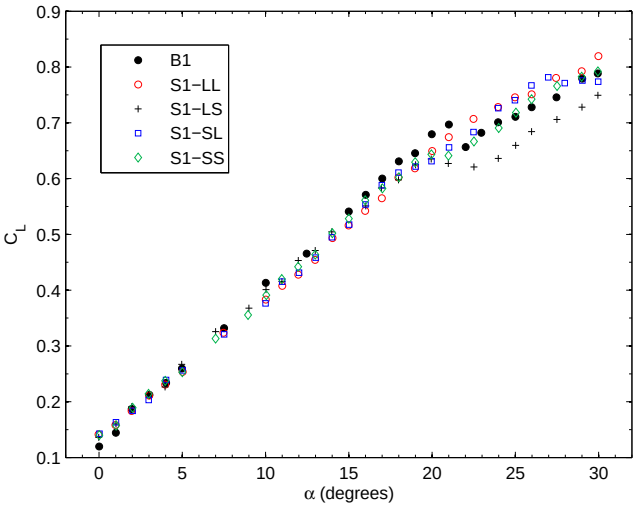


**Fig. 4 $C_L$ vs $\alpha$ for the models with $\mathcal{R} = 1$.**

**Table 3 Aerodynamic characteristics of the wings with aspect ratio 1.5.**

| Wing | $C_{L_{\alpha=0^\circ}}$ | $C_{L_{max}}$ | $\alpha_{C_{L_{max}}}$, deg | $\alpha_{stall}$, deg |
|---|---|---|---|---|
| B1.5 | 0.176 | 0.78 | 19 | 19 |
| S1.5-LL | 0.178 | 0.74 | 29 | 16 |
| S1.5-LS | 0.175 | 0.68 | 17 | 17 |
| S1.5-SL | 0.188 | 0.74 | 17 | 17 |
| S1.5-SS | 0.173 | 0.69 | 17 | 17 |

The baseline model $C_L$ increases at an approximately linear rate up to the angle of stall — $\alpha = 19^\circ$ —, where the maximum $C_L$ of 0.78 is reached. The stall is abrupt and severe. Flow visualization showed a leading edge stall. However, due to the reduced size of the bubble at this Reynolds number, we were unable to document it photographically. Further increases in angle of attack reduces the lift, but for $\alpha > 24^\circ$ it begins to augment. Aerodynamic hysteresis was found to be present. The hysteresis loop can be observed in Fig. 6 for the angles of attack lying between $17^\circ \leq \alpha \leq 20^\circ$. This results in considerable variations in lift coefficient. For example, the lift coefficient at $18^\circ$ at the increasing branch of the hysteresis loop was found to be 55% higher than at its decreasing branch.

The sinusoidal models present a lower (average) slope in the 'linear region'. Interestingly, now it is possible to observe that the S1.5-SL model — the one that is closer to the baseline leading edge geometry — has the highest slope among the sinusoidal models; while the others are kept indistinguishable. All sinusoidal models stall before the baseline model. However this is much softer and gradual. Additionally, its superiority at high angles of attack is unquestionable. Models of shorter wavelenght — S1.5-LS and S1.5-SS — behave in a similar fashion; they both stall at $\alpha = 17^\circ$ and after an initial reduction, the lift coefficient remains fairly constant. On the other side, the models of higher amplitude are the ones that generate superior gains (compared to the baseline). However, while the lift coefficient of S1.5-LL increases continuously between $19^\circ \leq \alpha \leq 29^\circ$ — reaching a maximum $C_L$ of 0.73, which is 9% higher than the $C_L$ at stall angle —, the model S1.5-SL suffers from an abrupt loss at $\alpha = 24^\circ$. No hysteresis was found to be associated with this loss of lift.

Note that, near the upper range of angles of attack studied, the rate of growth of lift is similar for both baseline and higher wavelength sinusoidal models.

The aerodynamic characteristics are listed in Table 3.

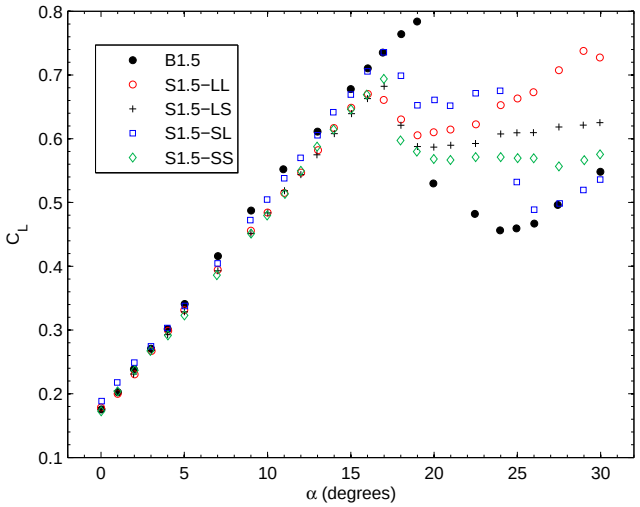


**Fig. 5 $C_L$ vs $\alpha$ for the models with $\mathcal{AR} = 1.5$.**

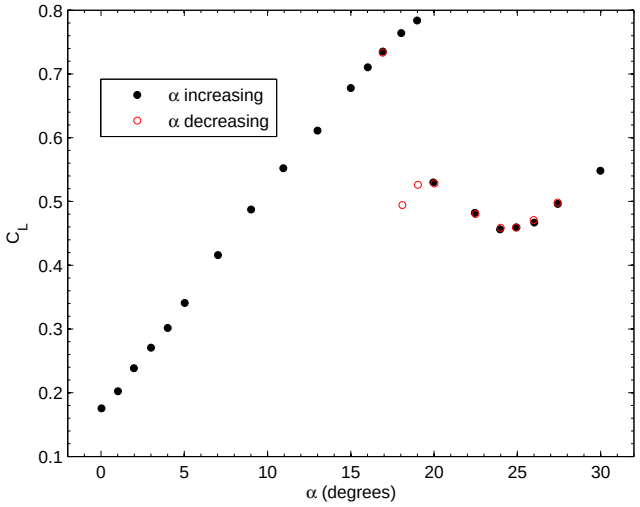


**Fig. 6 $C_L$ vs $\alpha$ for the baseline model with hysteresis loop.**

### 3. *Discussion*

For the wings with aspect ratio 1 there is no advantage in modifying the geometry of the leading edge. This is due to the absence of a truly stall behavior of the baseline model; the lift is only reduced in 6% and afterwards it starts increasing with incidence. In fact, the lift coefficient of all wings increases for high angles of attack. This trend can be typically found in low aspect ratio wings;[12,13] it is associated with the low pressure on the upper surface of the wing caused by the tip vortices. For LAR wings these vortices can have a dominant effect in the aerodynamic characteristics at high angles of attack. Torres and Mueller[13] also showed, by means of flow visualization, that the tip vortices energize the flow near the wingtips, limiting the separation bubble to the inboard section of the wing. So, this prevalent effect may explain the fast recovery of the baseline model from stall and the continuous increase of lift for all models, at high angles of attack. The lift coefficient of the S1-LL model normalized by the lift coefficient of the baseline model ($C_{L_{S1-LL}}/C_{L_{B1}}$) is plotted in Fig. 7. This clearly shows the superiority of the baseline model.

On the other hand, if we increase the aspect ratio the portion of the upper wing surface affected by the tip vortices is expected to decrease.

As a matter of fact, the baseline model of aspect ratio 1.5 presents a completely distinct stall behavior. The abrupt and severe stall causes a reduction of lift coefficient of 32% (from its maximum value). And in the poststall regime a proper combination of protuberances amplitude and wavelength — large amplitude and large wavelength — can lead to significant improvements over the baseline model. In Fig. 8 the normalized lift coefficient of the S1.5-LL model is plotted against angle of attack. Maximum gains of the order of 45% can be achieved with a maximum loss of about 20–25%.

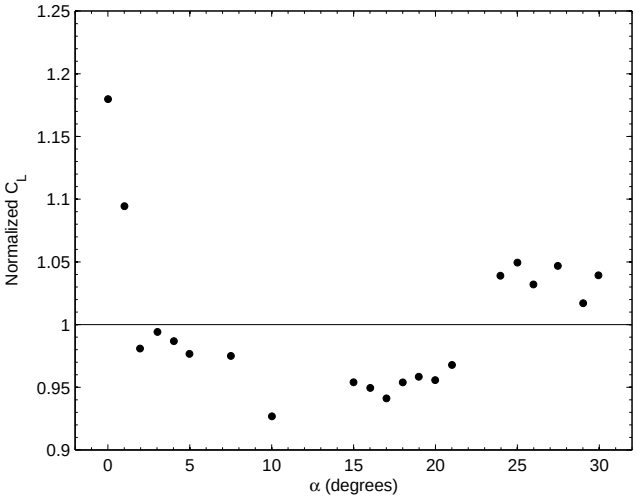


**Fig. 7 The S1-LL lift values normalized by the baseline lift values.**

The results of the wings with larger aspect ratio also show that both amplitude and wavelength play a major role in the evolution of lift coefficient; specially at high angles of attack. For a bidimensional experiment, the results from Johari et al.[9] showed that the wavelength played a minor role. However, if we compare the data evolution of S1.5-SL and S1.5-SS large differences can be appreciated in the post-stall regime.

*We also noted that the rate of growth of lift, for high angles of attack, is similar for these two sinusoidal models and the baseline model. This seems to indicate that there is some common mechanism responsible for that. If we think just in terms of the baseline model the logical response would be that the successive increase in incidence would increase the pressure difference between the lower an upper surface and thus intensify the tip vortices to a point that would reverse the trend of lift decrease. After some threshold angle of attack — here, approximately $\alpha = 24^\circ$ — the flow around the wing would be dominated by these structures and lift would start to increase continuously. For the sinusoidal models it seems that lift would be shaped by: a source of lift due to the protuberances vortices — that allow keeping $C_L$ at a higher level after stall —, a source from the tip vortices and the inevitable resulting interaction; which seems to be extremely favorable for the S1.5-LL model.*

## B. Low Reynolds Number

### 1. *Aspect ratio 1*

The lift coefficient vs angle of attack for all the wings with aspect ratio 1 is presented in Fig. 9. As can be clearly observed the wing models with protuberances along the leading edge have the potencial to generate large lift benefits across the range of angle of attack; specially for $0^\circ \leq \alpha \leq 5^\circ$.

The baseline model $C_L$ increases at highly non-linear rate up to the angle of stall, $\alpha = 19^\circ$. As was the case at moderate Reynolds number, it recovers immediately from stall — which reduces $C_L$ in only 5% — and the lift coefficient keeps increasing towards the maximum angle of attack. The maximum $C_L$ of 0.75 is 36% higher than the value at the stall angle.

The sinusoidal models in addition to the higher $C_L$ at low angles of attack have a more linear evolution, before the angle of stall of the baseline model. The model with large amplitude and large wavelength, in line with previ-

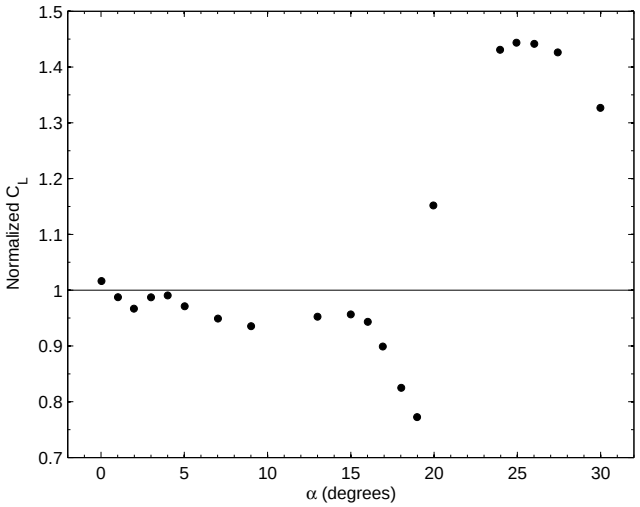


**Fig. 8 The S1.5-LL lift values normalized by the baseline lift values.**

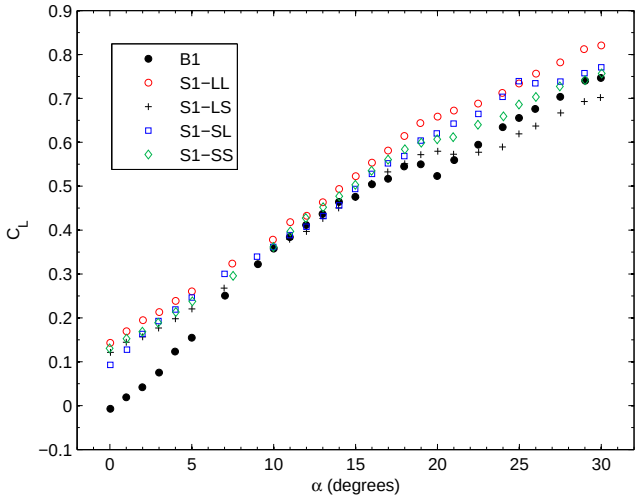


**Fig. 9 $C_L$ vs $\alpha$ for the models with $\mathcal{R} = 1$.**

**Table 4 Aerodynamic characteristics of the wings with aspect ratio 1.**

| Wing | $C_{L_{\alpha=0°}}$ | $C_{L_{max}}$ | $\alpha_{C_{L_{max}}}$, deg | $\alpha_{stall}$, deg |
|---|---|---|---|---|
| B1 | -0.007 | 0.75 | 30 | 19 |
| S1-LL | 0.143 | 0.82 | 30 | – |
| S1-LS | 0.121 | 0.70 | 30 | 20 |
| S1-SL | 0.093 | 0.77 | 30 | – |
| S1-SS | 0.130 | 0.76 | 30 | – |

ous results, has notable aerodynamic characteristics, and the lift advantages against the baseline model are only reduced in the range of $10° \leq \alpha \leq 15°$. This is because of the lower average slope in the prestall regime, nonetheless the superiority is evident. The S1-LS model as the lowest performance among the sinusoidal models; this is consistent with previous results.

The aerodynamic characteristics are listed in Table 4.

### 2. *Aspect ratio 1.5*

The lift coefficient for the wings with aspect ratio 1.5 is plotted in Fig. 10 as a function of angle of attack. Again, the sinusoidal models have the potential to generate large lift benefits; specially for $0° \leq \alpha \leq 5°$ and $17° \leq \alpha \leq 30°$.

The baseline model $C_L$ increases at a non-linear rate up to the angle of stall at 16°, where the maximum $C_L$ of 0.64

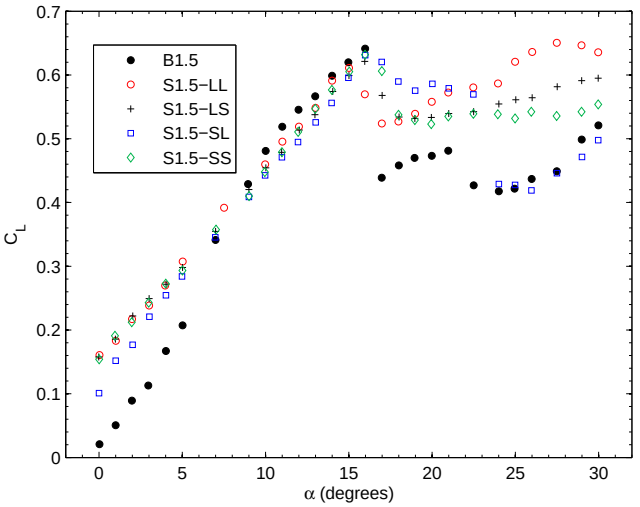


**Fig. 10 $C_L$ vs $\alpha$ for the models with $\mathcal{R} = 1.5$.**

**Fig. 11 Flow visualization of the B1.5 model at stall angle. Note the laminar separation bubble near the leading edge.**

**Table 5 Aerodynamic characteristics of the wings with aspect ratio 1.5.**

| Wing | $C_{L_{\alpha=0°}}$ | $C_{L_{max}}$ | $\alpha_{C_{L_{max}}}$, deg | $\alpha_{stall}$, deg |
|---|---|---|---|---|
| B1.5 | 0.021 | 0.64 | 16 | 16 |
| S1.5-LL | 0.161 | 0.65 | 27.5 | 15 |
| S1.5-LS | 0.158 | 0.62 | 16 | 16 |
| S1.5-SL | 0.101 | 0.63 | 16 | 16 |
| S1.5-SS | 0.154 | 0.63 | 16 | 16 |

is reached. The abrupt stall causes a reduction in lift coefficient of approximately 32%. However, no aerodynamic hysteresis was found at this lower Reynolds number. Flow visualization showed a leading edge stall that can be appreciated in Figs. 11 and 12. After stall, $C_L$ increases up to $\alpha = 21°$, where a further reduction takes place. For $\alpha \geq 25°$, the evolution is quite similar to the one at higher Reynolds number, depicted in Fig. 5.

The sinusoidal models present a lower (average) slope — but more linear — before the stall angle; the S1.5-SL has the highest slope among the models with protuberances. The stall is more gradual and less severe, leading to an improved performance in the poststall regime. While at higher Reynolds numbers all sinusoidal models stalled first, at low Reynolds number only the S1.5-LL stalls before the baseline model, at 15°. In the poststall regime, the lift coefficient evolution with angle of attack is identical to the $Re = 140000$.

The aerodynamic characteristics are listed in Table 5.

### 3. *Discussion*

For the wings with aspect ratio 1 and contrary to the results at moderate Reynolds number it would be advantageous —

**Fig. 12 Flow visualization of the B1.5 model, one degree after stall angle. Note the flow completely separated.**

in terms of lift coefficient — to use a sinusoidal leading edge. The lift of the model with large amplitude and large wavelenght protuberances is higher throughout the all range. In Fig. 8 the normalized lift coefficient of this model is plotted against angle of attack, for $\alpha \geq 10^{\circ}$. We only plot the data for $\alpha \geq 10^{\circ}$ because the large diference between the values at low angles of attack plus the low values of the baseline model lift coefficient would preclude a proper visualization. The results for higher Reynolds number are also plotted to enrich the analysis. Maximum gains of the order of 25% can be obtained for $\alpha \geq 10^{\circ}$; remember that for lower angles the gains are much higher.

To understand the cause of such differences in Figs. 14 and 15 we plot the lift coefficient against angle of attack at moderate and low Reynolds number, for the baseline and S1-LL model, respectively. As can be seen the decrease in Reynolds number leads to a substancial performance deterioration of the baseline model, particularly at low angles of attack, while the S1-LL seems to be remarkably insensitive to this Reynolds number variation. This is due to a significant region of separated flow near the trailing edge of the baseline model at $Re = 70000$, which is smaller or nonexistent for the sinusoidal models. This will be analyzed in more detail with the aid of flow visualization, for the models with aspect ratio 1.5.

The performance deterioration of the baseline model also translates in a lower stall angle. Interestingly, the maximum $C_L$ is only reduced in 5%. This is due to the higher average slope after stall angle. *This behavior may result from an increase in the tip vortices strength caused by the increase in viscous effects associated with the decrease in Reynolds number (check with flow visualization).*

For the wings with aspect ratio 1.5, the baseline model is also quite more sensitive to Reynolds number decrease as can be concluded by comparing Figs. 16 and 17. The first plots $C_L$ vs $\alpha$ at moderate and low Reynolds numbers for the baseline model, and the second for the S1.5-LL model.

The lift coefficient of the baseline model is reduced, mainly for $0^{\circ} \leq \alpha \leq 5^{\circ}$; analogous to the results at lower aspect ratio. Now, this is easily understood by analyzing and comparing Figs. 18 and 19, which illustrate the behavior of the boundary layer at $\alpha = 3^{\circ}$, respectively, for moderate and low Reynolds numbers. As can be seen, the boundary layer separates near the trailing edge in both cases. However, at moderate Reynolds number it reattaches to the surface forming a bubble, while at low Reynolds number the separated shear layer can no longer reattach to the surface. Additionally, flow visualization of the S1.5-LL model showed the formation of a small bubble, completely negligible if compared with the previous ones, and so impossible to document photographically. Thus, we can also understand the lower sensitivity of these models to Reynolds number. Another interesting note is that the sinusoidal model closer

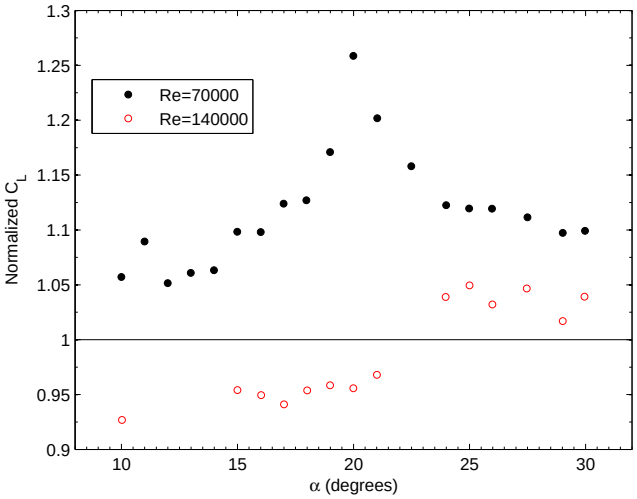


**Fig. 13 The S1-LL lift values normalized by the baseline lift values.**

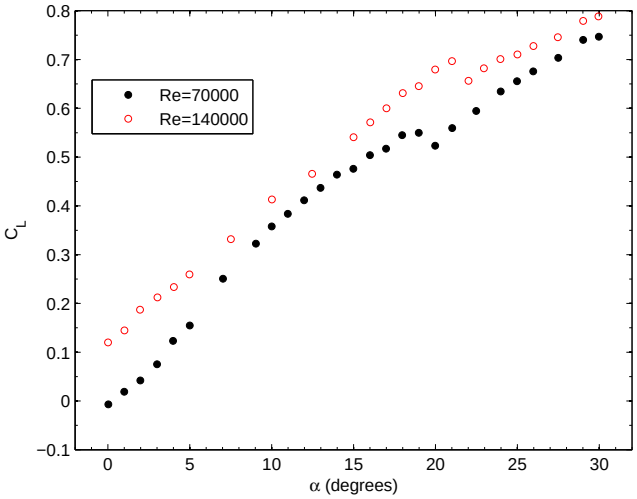


**Fig. 14 $C_L$ vs $\alpha$ for the B1 model at Reynolds number of 70000 and 140000.**

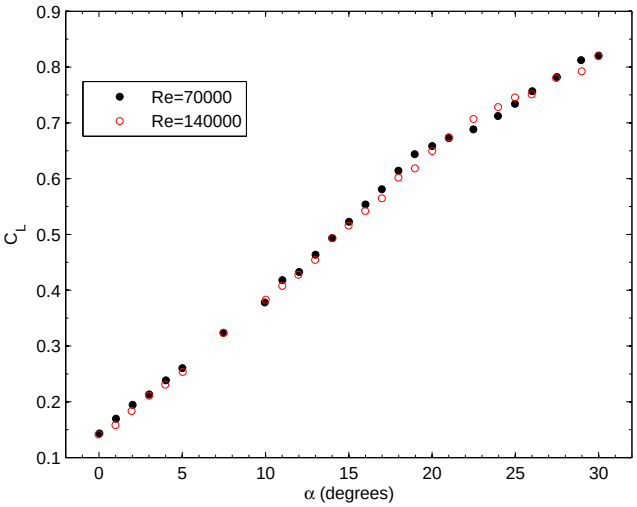


**Fig. 15 $C_L$ vs $\alpha$ for the S1-LL model at Reynolds number of 70000 and 140000.**

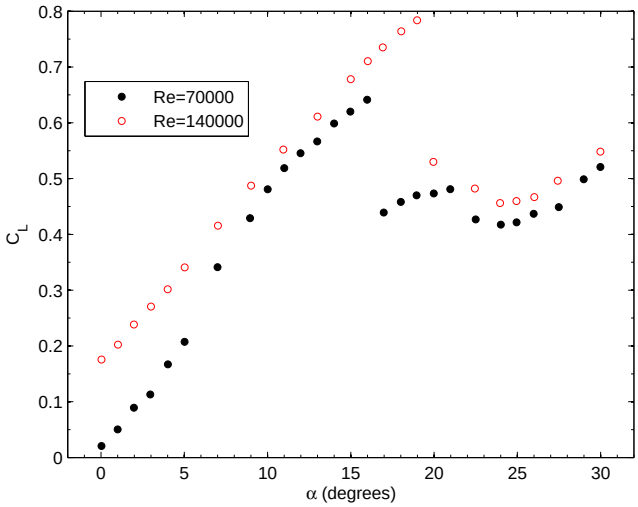


**Fig. 16 $C_L$ vs $\alpha$ for the B1.5 model at Reynolds number of 70000 and 140000.**

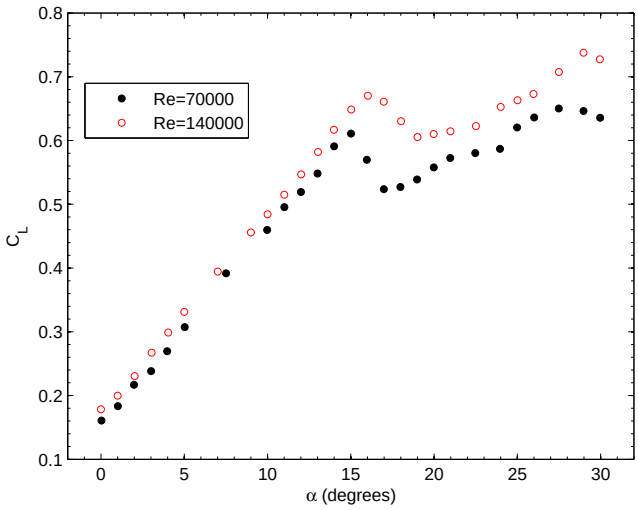


**Fig. 17 $C_L$ vs $\alpha$ for the S1.5-LL model at Reynolds number of 70000 and 140000.**

to the baseline model (S1.5-SL) is more affected by the Reynolds number reduction at low angles of attack (review Fig. 10); this can also be seen for the higher Reynolds number, but to a lower extent.

The effective benefits of using a sinusoidal leading edge with large amplitude and wavelength can be appreciated in Fig. 20, where the normalized lift coefficient is plotted as a function of angle of attack at low and moderate Reynolds numbers, for $\alpha \geq 10°$; again we must not forget the benefits accomplished at low angles of attack. For $\alpha \geq 10°$, maximum $C_L$ improvements of 45% over the baseline model can be obtained with an average penalization of approximately 5% in the range $10° \leq \alpha \leq 16°$. The maximum overall penalization of the order of 10% at $\alpha = 16°$ is about half the maximum penalization at the higher Reynolds number.

## IV. Conclusions

The aerodynamic characteristics of wings with low aspect ratio, rectangular planforms, and sinusoidal leading edges, were studied through a series of wind tunnel tests and compared with the results of a baseline model. Of primary interest were the effects of aspect ratio, leading edge geometry, and Reynolds numbers on the lift forces. The amplitude of leading edge protuberances were 6% and 12% of the mean chord length and the wavelength were 25% and 50% of the mean chord length.

At higher Reynolds numbers the protuberances cause a reduction in lift coefficient for angles of attack below the

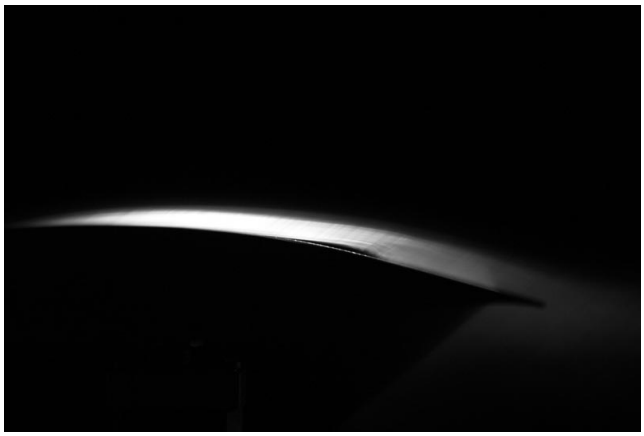

**Fig. 18 Flow visualization of the B1.5 model at Re=140000, $\alpha = 3°$.**

**Fig. 19 Flow visualization of the B1.5 model at Re=70000, $\alpha = 3°$.**

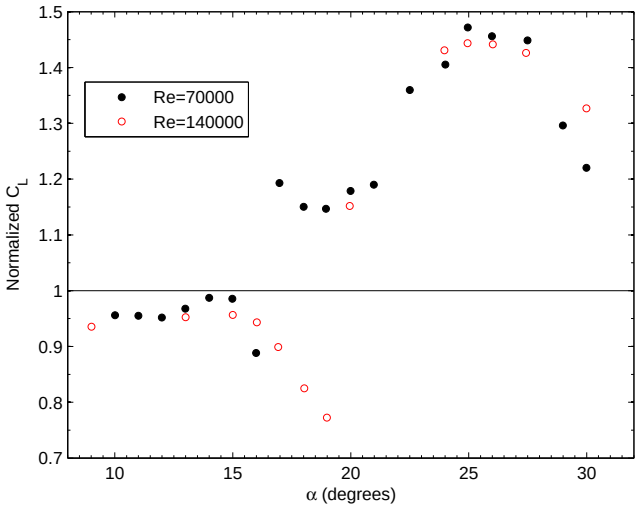


**Fig. 20 The S1.5-LL lift values normalized by the baseline lift values.**

baseline model stall angle. For $\alpha \geq \alpha_{stall}$, the results depend strongly in the aspect ratio. For wings with aspect ratio 1.5, the sinusoidal models have a much softer stall than the baseline model and its possible to achieve maximum lift coefficient gains of the order of 45%; plus, they eliminate the aerodynamic hysteresis associated with the abrupt and severe baseline model stall. In turn, the baseline model with aspect ratio 1, by action of the tip vortices (more influent at lower $AR$), experience only a slight loss of lift accompanied by a continuously increase in lift up to the maximum angle of attack. Thus the losses introduced by the protuberances overcome the gains.

The decrease in Reynolds number has significantly different effects in the wings with and without protuberances. If on one hand, the wings with protuberances are fairly insensitive to the variation of Reynolds number, on the other hand, the lift coefficient performance of the baseline models is considerably deteriorated. This leads to an overall increase of the beneficial effects of the sinusoidal models; specially at low angles of attack. So one can say that sinusoidal leading edge lifting surfaces are less prone to performance deterioration. This is the most important result of our study, because in any project the ultimate goal is to achieve a stable and controlled flight with the maximum aerodynamic efficiency throughout the entire range of operation.

The results also indicate that both the amplitude and wavelength of protuberances play an important role on the resulting forces.

## References

[1]Mueller, T.J., "Aerodynamic Measurements at Low Reynolds Numbers for Fixed Wing Micro-Air Vehicles," *Proceedings of the Development and Operation of UAVs for Military and Civil Applications Short Course*, Belgium, September 13–17, 1999, published in Rto-EN-9 by NATO, April 2000.

[2]Ettinger, S.M., Nechyba, M.C., Ifju, P.G., and Waszak, M., "Vision-Guided Flight Stability and Control for Micro Air Vehicles," Intelligent Robots and Systems, IEEE/RSJ International Conference, 2002.

[3]Al-Qadi, I.M., and Al-Bahi, A.M., "Micro Aerial Vehicles Design Challenges: State of The Art Review," *SSAS UAV Scientific Meeting & Exhibition*, Jeddah, Saudi Arabia, 2006.

[4]Woodward, B.L., Winn, J.P., and Fish, F.E., "Morphological Specializations of Baleen Whales Associated With Hydrodynamic Performance and Ecological Niche," *Journal of Morphology*, Vol. 267, No. 11, Nov. 2006, pp. 1284–1294.

[5]Fish, F.E., and Battle, J.M., "Hydrodynamic Design of the Humpback Whale Flipper," *Journal of Morphology*, Vol. 225, No. 1, Nov. 1995, pp. 51–60.

[6]Miklosovic, D.S., Murray, M.M., Howle, L.E., and Fish, F.E., "Leading-Edge tubercles Delay Stall on Humpback whale (Megaptera Novaeangliae) Flippers," *Physics of Fluids*, Vol. 16, No. 5, May 2004, pp. 39–42.

[7]Stanway, M.J., *Hydrodynamic Effects of Leading-Edge Tubercles on Control Surfaces and in Flapping Foil Propulsion*, Master of science in ocean engineering, Massachusetts Institute of Technology, Feb. 2008.

[8]Miklosovic, D.S., Murray, M.M., and Howle, L.E, "Experimental Evaluation of Sinusoidal Leading Edges," *Journal of Aircraft*, Vol. 44, No. 4, 2007, pp. 1404–1407.

[9]Johari, H., Henoch, C., Custodio, D., and Levshin, A., "Effects of Leading-Edge Protuberances on Airfoil Performance," *AIAA Journal*, Vol. 45, No. 11, 2007, pp. 2634–2642.

[10]Pedro, H.T.C., and Kobayashi, M.H., "Numerical Study of Stall Delay on Humpback Whale Flippers," *AIAA Paper 2008-584*, Jan. 2008.

[11]Coleman, H.W., and Steele, W.G., "Engineering Application of Experimental Uncertainty Analysis," *AIAA Journal*, Vol. 33, No. 10, 1995, pp. 1888–1896.

[12]Torres, G.E., and Mueller, T.J., "Low-Aspect-Ratio Wing Aerodynamics at Low Reynolds Numbers," *AIAA Journal*, Vol. 42, No. 5, 2004, pp. 865–873.

[13]Torres, G.E., and Mueller, T.J., "Aerodynamic Characteristics of Low Aspect ratio Wings at Low Reynolds Numbers," *Fixed and Flapping Wing Aerodynamics for Micro Air Vehicle Applications*, edited by T. Mueller, Vol. 195 of *Progress in Astronautics and Aeronautics*, AIAA, Reston, 2001, pp. 115–141.